Aeroelastic design of a drone for research on active flutter control

Nicolò Fabbiane, Vincent Bouillaut, Arnaud Lepage

International Forum on Aeroelasticity and Structural Dynamics
IFASD 2024
17-21 June 2024, The Hague, The Netherlands

AEROELASTIC DESIGN OF A DRONE FOR RESEARCH ON ACTIVE FLUTTER CONTROL

Nicolò Fabbiane[1], Vincent Bouillaut[1], Arnaud Lepage[1]

[1]DAAA, ONERA, Institut Polytechnique de Paris,
29 Av. de la Division Leclerc, 92320 Châtillon, France
nicolo.fabbiane@onera.fr
vincent.bouillaut@onera.fr
arnaud.lepage@onera.fr

Keywords: aeroelastic tailoring, flutter, flying demonstrator.

Abstract: Within the project CONCERTO, funded by the European research program Clean Aviation, ONERA is responsible of the aeroelastic design of a flying demonstrator, aimed at providing a suitable platform for the test of active control techniques to delay the onset of the flutter instability. This leads to very peculiar specifications for the nominal flutter behaviour of the aircraft and, therefore, to adapted solutions in the design process. The flutter behaviour of the drone has to be adjustable; in particular, three configurations are expected. First, a reference configuration is required without any flutter occurrence in the flight domain and any coupling between flight mechanics and structural dynamics. For the second one, the first flexible mode's frequency is low enough to interact with the flight dynamics, still being flutter stable. Finally, the third one presents a flutter instability for a specific range of velocities in the flight domain. Thus, the design has to include a way to tune separately the flexional and torsional natural vibration modes of the wing. To this end, a system of movable masses positioned at the tip of the wing is introduced, providing the degrees of freedom to pilot the structural dynamic and, hence, the aeroelasticity of the drone. Along these design parameters, the wing structure is also tailored to ensure the necessary sensitivity of the structural dynamics to the above-mentioned movable masses. This paper summarises the design process: starting from the baseline structural configuration, some structural parameters are tuned to comply with the above-mentioned specifications. Finally, a thorough analysis of the (linear) aeroelastic behaviour is presented, to verify and document the expected performance of the drone.

1 INTRODUCTION

Aeronautics has long dealt with balancing structural weight and flexibility. A light structure was necessary for flight, yet rigidity was essential to prevent undesirable interactions with aerodynamics. However, the research and engineering community soon realised that these interactions could be beneficial — or at least controlled – in terms of aeronautical performance [1]. This approach became known as *aeroelastic tailoring* and has been an integral part of the aeronautical design process in recent decades [2, 3], especially with the advent of composite materials in aeronautical structures, e.g. [4–6].

A common application of aeroelastic tailoring is the suppression or delay of flutter instability [7]. Flutter is classically defined as an aeroelastic instability resulting from the interaction of two structural modes through the airflow, allowing them to couple and combine into two

Figure 1: Artistic view of CONCERTO's Experimental Validation Aircraft (EVA). Courtesy of Aviation Design.

aeroelastic modes, with one becoming unstable at a particular flight speed, known as the "critical flutter velocity" [8]. Therefore, the objective of a classical design procedure is to push the onset of flutter outside of the flight domain, i.e., the range of velocities and altitudes for which an aircraft is certified. Research in this field has expanded to consider uncertainty in structural properties in the design process to achieve robust [9] and/or reliable [10, 11] design points.

Sometimes, optimising the structure alone is neither sufficient nor possible, and active control techniques must be employed to suppress flutter [12]. This has sparked a research field focused on developing control laws and demonstrating their effectiveness [13], with numerous dedicated research projects emerging in recent years [14–16].

To experimentally test these techniques, a flying test-bench with precise and well-understood flutter behaviour must be designed. This is essential to ensure the safety of experimental campaigns and to provide a controlled environment for scientifically relevant results. In this context, aeroelastic tailoring techniques—traditionally employed to prevent flutter—are used to design aircraft that are intentionally flutter-unstable. These aircraft serve as suitable platforms for demonstrating active flutter suppression technologies [16]. This study operates within this framework.

Within the Clean Aviation project CONCERTO, Dassault Aviation, Aviation Design and ONERA develop an Experimental Validation Aircraft (EVA) – see Figure 1 – to test active control techniques for the control of the flutter instability[1]. The objective of this work is the aeroelastic design of the EVA with the aim of satisfying the peculiar specifications that come from its mission (§ 2). The baseline configuration of the aircraft is introduced and characterised, as well as the design parameters (§ 3). Thus, the aeroelastic design process is outlined by means of parametric studies on the design variables (§ 4). Finally, the design is identified and its aeroelastic requirements are verified (§ 5).

[1] www.youtube.com/watch?v=gbenJtp0Ybo

2 OBJECTIVES AND SPECIFICATIONS

The overall objective is the design of a drone for the study of active flutter control and controllability of a flexible aircraft whose first elastic modes are close to the flight mechanics ones. This leads to very peculiar specifications for the aircraft; if in a conventional aeroelastic structural design the main objective is to avoid flutter, in this work we not only aim for flutter to occur in the flight domain, but also to pilot when and how. Additionally, other constraints on the natural frequencies of the EVA are in place to control the interaction with the flight dynamics.

Hence, three configurations are required, in order to gradually approach the occurrence of aeroelastic phenomena and coupling:

- a *rigid* configuration, with a conventional flutter constraint and a first natural frequency high enough to weakly couple with the flight dynamic;
- a *flexible* configuration, still with a conventional flutter constraint but a first natural frequency low enough to strongly couple with the flight dynamic;
- a *flutter* configuration, with the onset of flutter in the flight domain, preferably with a mechanism involving symmetric structural modes.

The details of the specific requirements for each configuration are reported in Table 1. The reported values are all to be considered at the ground level, since all the flight tests will be conducted at very low altitude. These three configurations should possibly share the same wing structure and the different behaviours should be obtained by adjustable elements that can be set on the ground before each flight. Moreover, the specifications on the flutter behaviour should be guaranteed for a value of modal damping of 1.5%.

Table 1: Dynamical and flutter specifications for the three required configurations.

Label	Lowest natural freq. (f_1^n)	Critical flutter speed (TAS^*)
rigid	$f_1^n \approx 5\,\text{Hz}$	$TAS^* > 1.2 \times VNE = 300\,\text{km/h}$
flexible	$f_1^n \approx 3\,\text{Hz}$	$TAS^* > 1.2 \times VNE = 300\,\text{km/h}$
flutter	$f_1^n \approx 3\,\text{Hz}$	$175\,\text{km/h} < TAS^* < 225\,\text{km/h}$

Furthermore, classical aeroelastic constraints on the aeroelastic deformation, static divergence, and control reversal of the wing are also enforced. The former to ensure that the aerodynamic design of the wing is not largely affected by its static aeroelastic behaviour: an aeroelastic twist of at most 1° has to be ensured in cruise conditions, while no real limit is prescribed on the vertical tip displacement other than inherent structural requirements. The latter is set to ensure the in-flight controllability of the EVA throughout the test campaign: sufficient effectiveness is required in the flight domain, with no control reversal in the extended one. This specification is of particular importance since the active flutter control is expected to be performed via one of the ailerons.

3 THE EXPERIMENTAL VALIDATION AIRCRAFT (EVA)

The Experimental Validation Aircraft (EVA) is an unmanned, remote-controlled aircraft and, as introduced above, it is meant to be a demonstrator for the active control of the flutter instability. Its design is a collaborative work between Dassault Aviation, ONERA, and Aviation Design, the latter being responsible also for its manufacturing. It presents a classical T-tail configuration, with two small turbine engines mounted on the fuselage and a non-retractable gear. The max take-off weight is limited to by the safety parachute, with an aspect ratio of approximately 15

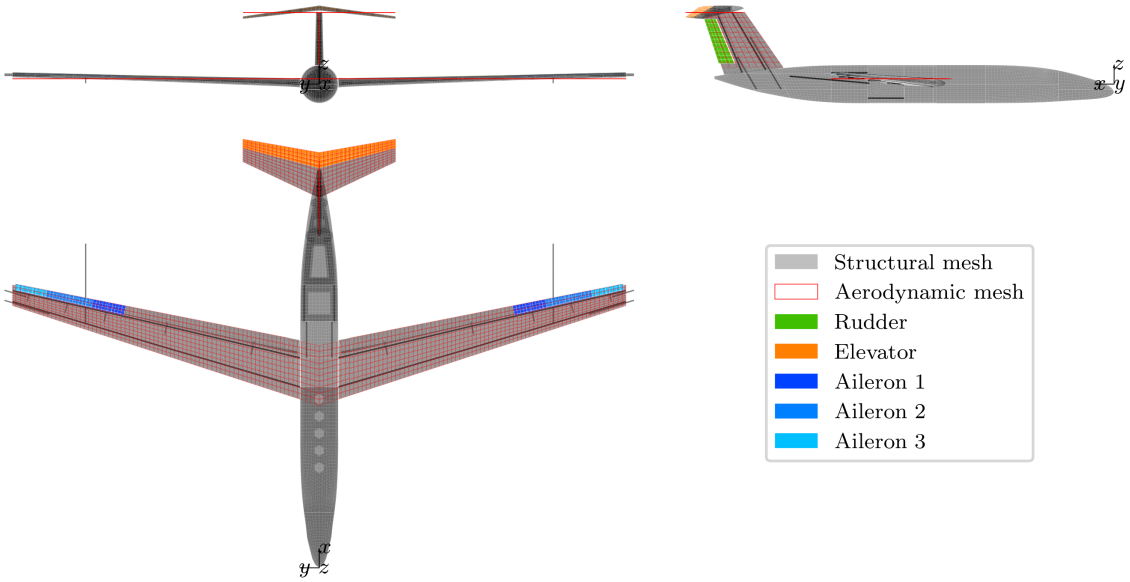

Figure 2: Three-sides view of the structural and aerodynamic meshes of the EVA. The control surfaces (rudder, elevator, and ailerons) are highlighted by the colours.

and a target velocity not-to-exceed (VNE) of 250 km/h. Elevator and rudder control surfaces ensure the manoeuvrability along the pitch and yaw axes, while three independent ailerons for each wing control the movement along the roll axis (see Figure 2). Each control surface is piloted by an independent electrical actuator.

The structure of the EVA is mainly made of composite materials, with only some some parts in steel and aluminium (fuselage frames and wing-fuselage connections). An aeroelastic model representative of the drone has been created in MSC NASTRAN [17], based on the technical drawings by Aviation Design. The structural model counts approximately 40 000 plate and 2 000 bar elements, which model the principal components of the overall primary structure. The control surfaces and their connection to the wing/tail structure are independently meshed, allowing the model to be representative of their aeroelastic behaviour. The aerodynamic is modelled via the doublet-lattice-method native to MSC NASTRAN: the coupling between aerodynamic and structure is made on the spars of the wing, the tail, and the control surfaces via an infinite-plate kinematic. A three-sides view of the structural and aerodynamic meshes of the EVA is reported in Figure 2.

3.1 Design parameters: adjustable masses and ply angle

The initial design of the EVA already implemented some adjustable parameters in the structure. These consist in tunable masses in placed in the wing, at each wing-tip (m_{tip}) in the pods visible in Figure 1 and at the end of a rear-facing beam (m_{ft}) at approximately three quarters of the wing span. The latter will be indicated from now on as "flutter tuner", since they will have a primary role in tuning the flutter characteristics of the wing (see § 4.3). While these are fixed in position, the masses in the pods can be placed at a certain distance (d_{tip}) with respect to the centre of the pod, which coincides with the mid-point between the spars. For the present study, we will consider only symmetric cases – i.e. with the two masses placed at the same distance from the centre – even if the design would allow the masses to be placed independently from each other. Figure 3 shows the placing of the masses with respect to the wing, as well as the other design parameters that are described in the following.

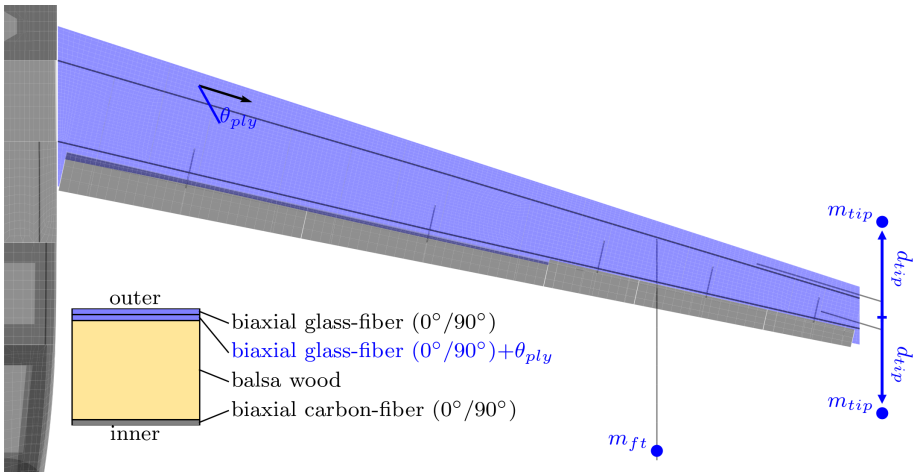

Figure 3: Design parameters for the EVA's wing: tip masses (m_{tip}), distance between the tip masses (d_{tip}), flutter-tuner mass (m_{ft}), and orthotropy angle (θ_{ply}) of the inner glass-fibre ply.

An additional design parameter is given by the orientation angle (θ_{ply}) of the mid-ply in the composite stack of the wing skin. As reported in the left bottom corner of Figure 3, it is made by a composite sandwich, composed from the inner to the outer layer of one ply of biaxial carbon-fibre, one ply of balsa wood – to facilitate the geometry control during the fabrication process –, and two plies of biaxial glass-fibre. The fibres of the most external plies are oriented parallel and perpendicular with respect to the bow spar; the mid glass-fibre ply, instead, has an angle θ_{ply} with respect to the same direction. Note that the positive sign of the orientation is given by the wall-normal direction of the wing surface, i.e. it inverts direction between pressure and suction side. This will allow us to pilot the stiffness distribution between flexion and torsional behaviour of the wing, as we will show in § 4.2.

3.2 Baseline configuration

The baseline for this study is the initial design proposed by Aviation Design. It considers all the support structure for the adjustable masses – with no masses – and a mid-ply angle $\theta_{ply} = -45°$.

The modal analysis of this configuration resulted in the natural modes reported in Table 2; a more visual representation of the modes is available in Figure 4. The first flexion mode of the wing ($W_{f,1}$) is found to be the first natural mode of the aircraft, with a frequency of 4.55 Hz, not far from the 5 Hz prescribed by the specifications for the rigid configuration (see Table 1). The two torsion modes ($W_{t,s}$ and $W_{t,a}$) appear approximately at the same frequency of approximately 17 Hz: this is due to the high rigidity of the fuselage and the way the two wings are connected to it, without a direct connection between the two spars. They sit after the second flexion mode and between the two co-planar ones, and this will have an effect on the flutter characteristic of this configuration. No clear modes of the flutter tuner are observed.

The native implementation of the pk-method [18] in MSC NASTRAN is used to solve the eigenvalue problem of the classical flutter equation:

$$\mathbf{M}\ddot{\mathbf{q}} + (\mathbf{K} + \mathbf{K}_a(TAS, f))\,\mathbf{q} = \mathbf{0},$$

where $\mathbf{q}$ is the vector of the structural degrees of freedom, $\mathbf{M}$ the structural mass matrix, $\mathbf{K}$ the structural rigidity matrix, and $\mathbf{K}_a$ the aerodynamic rigidity matrix, which is a function of the flight speed (TAS) and the coupled modal frequency (f). The frequency and the damping ratio

Table 2: Organisation of the natural vibration modes of the baseline configuration.

Label	freq. (Hz)	Description
$W_{f,1}$	4.55	1st flexion mode of the wing (symmetric)
$W_{f,2}$	9.25	2nd flexion mode of the wing (antisymmetric)
$W_c + V_t$	15.8	co-planar mode of the wing + torsional mode of the VTP
$W_{t,s}$	17.2	symmetric torsional mode of the wing
$W_{t,a}$	17.3	antisymmetric torsional mode of the wing
$W_c + V_f$	18.2	co-planar mode of the wing + flexion mode of the VTP
$W_{f,3}$	21.0	3rd flexion mode of the wing (symmetric)
$FT_{f,s}$	–	symmetric flexion mode of the flutter tuner.
$FT_{f,a}$	–	antisymmetric flexion mode of the flutter tuner.

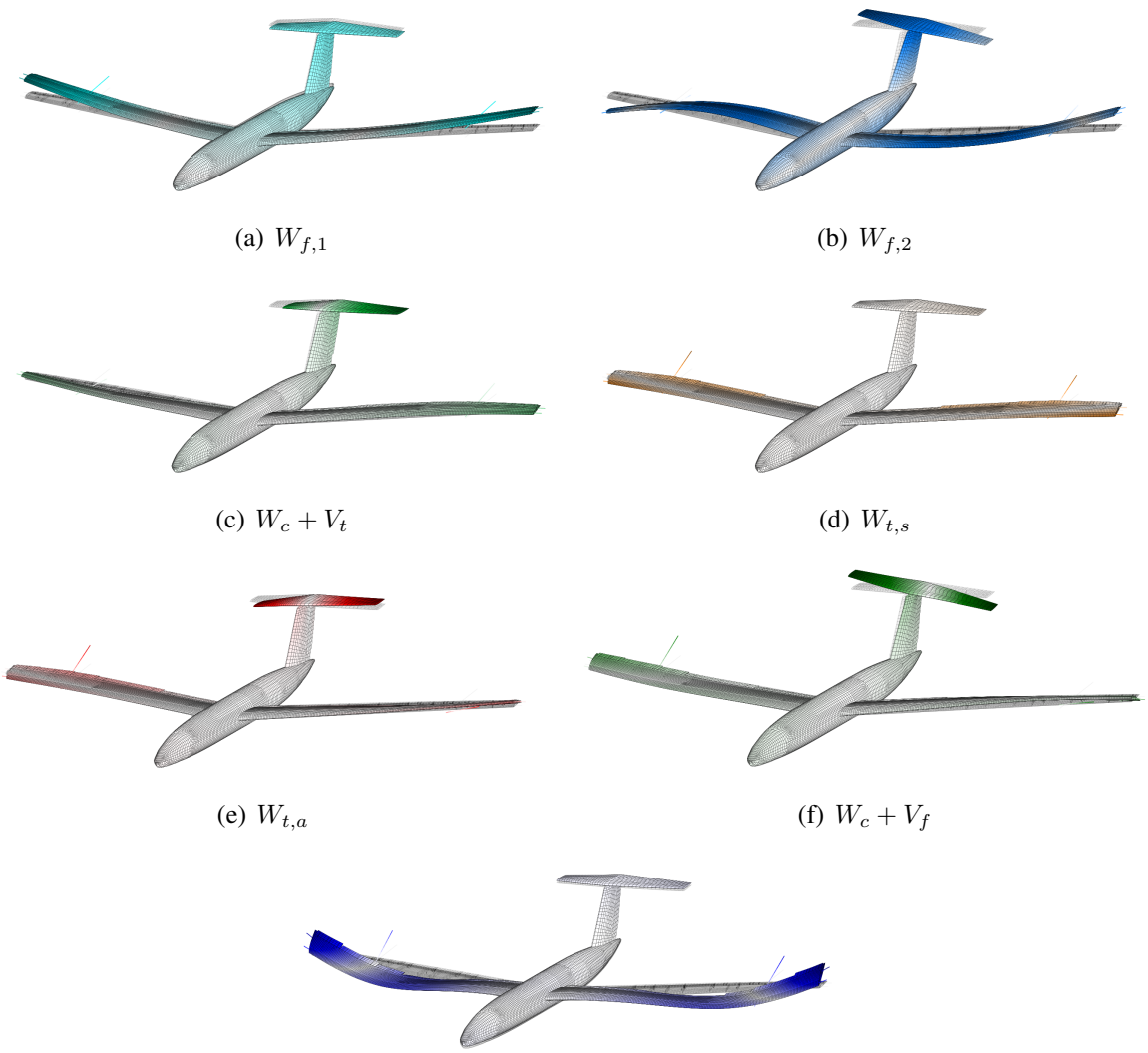

(a) $W_{f,1}$ (b) $W_{f,2}$

(c) $W_c + V_t$ (d) $W_{t,s}$

(e) $W_{t,a}$ (f) $W_c + V_f$

(g) $W_{f,3}$

Figure 4: Modal shapes of the baseline configuration, see Table 2 for labelling.

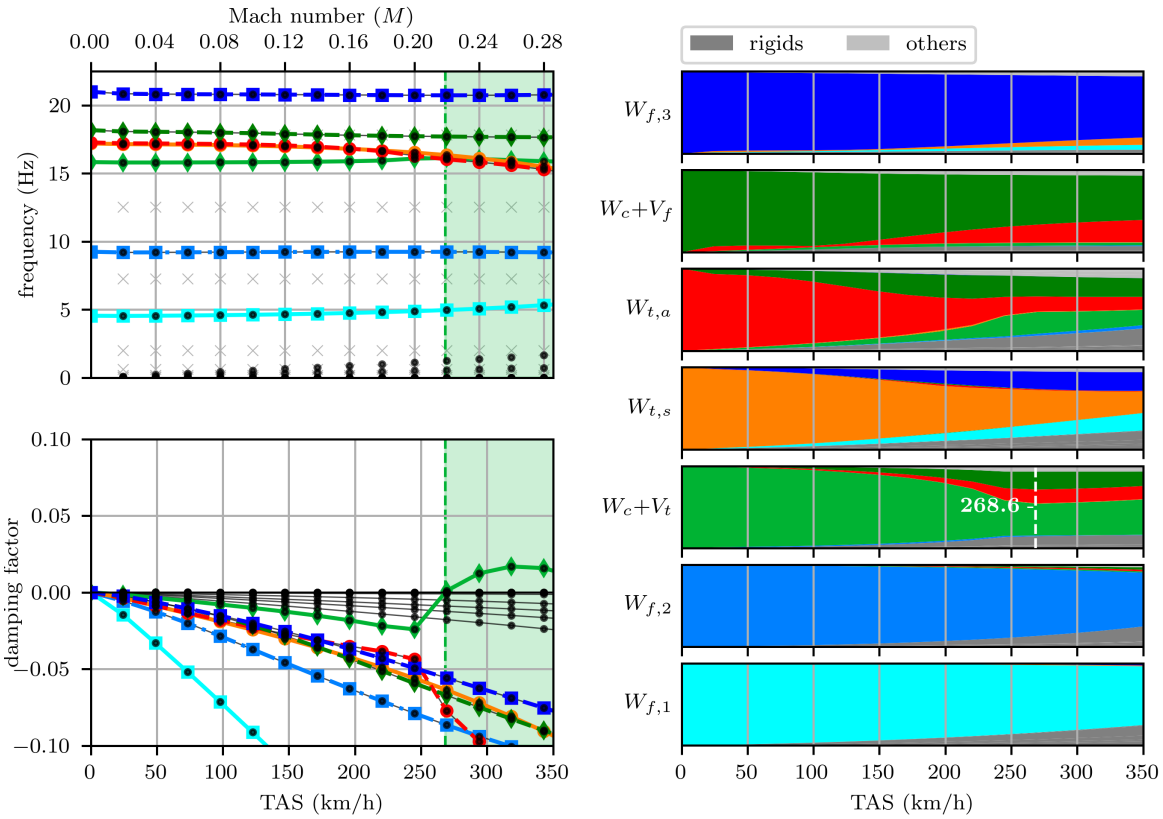

Figure 5: Baseline: flutter diagram and modal contributions.

– defined as the ratio between the real and imaginary part of the coupled eigenvalue – are reported as a function of the flight speed in Figure 5(left). Each mode is followed with a maximal resemblance criterion between two consecutive flight speeds, and the labelled modes are highlighted with colours. The critical flutter velocity (TAS^*) is defined as the lowest velocity for which the damping ratio becomes positive. Thus, the flutter analysis predicts a critical velocity $TAS^* = 268.8$ m/s, lower than the limit value of $1.2 \times VNE = 300$ km/h for the two flutter-less configuration. Figure 5(right) shows the modal components of the coupled eigenvalues for the tracked modes; the flutter mechanism of the baseline configuration sees the coupling of the two co-planar modes with the antisymmetric wing torsion. The dark grey area at the bottom of each plot indicates the contribution of the rigid modes. This analysis is very useful in the following design section to ensure a symmetric flutter mechanism.

4 AEROELASTIC DESIGN

This section presents the aeroelastic design of the EVA by means of parametric studies aimed to identify a suitable set of the parameters (§ 3.1) that complies with the specifications (§ 2).

We first address the requirements on the lowest natural frequency by tuning the adjustable masses in the pods at the tip of the wing (§ 4.1). Then, their position and the ply angle are adjusted to obtain the onset of the flutter within the flight domain with the desired symmetric mechanism (§ 4.2). Finally, the flutter behaviour is fine tuned via the flutter tuner masses (§ 4.3).

4.1 Lowest natural frequency (tip masses)

The main role of the masses added in the pods at the wing-tip is to pilot the lowest natural frequency of the aircraft, i.e. the first flexion mode of the wing. Starting from the baseline

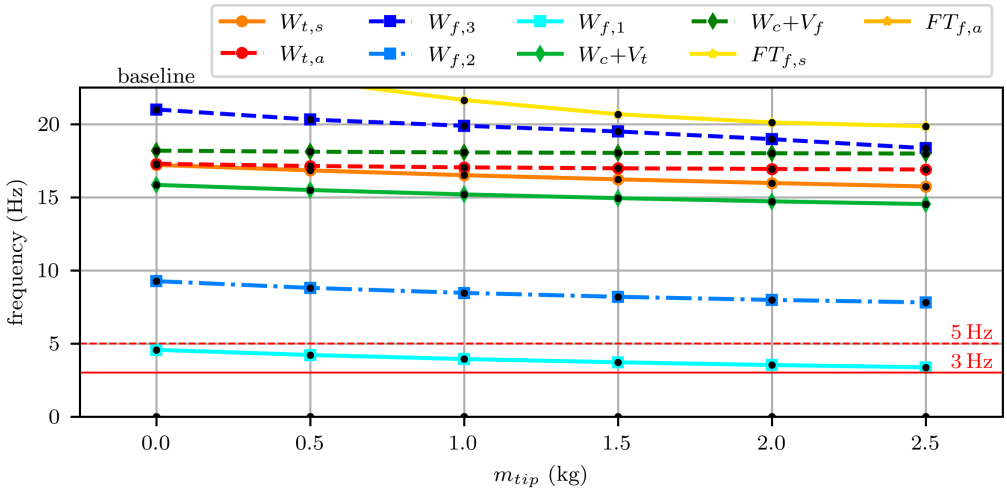

Figure 6: Parametric study on the mass at the wing-tip (m_{tip}). The values of the other design parameters are: $\theta_{ply} = -45°$, $d_{tip} = 0\,\text{m}$, and $m_{ft} = 0\,\text{kg}$.

configuration, Figure 6 reports the evolution of the natural frequencies for increasing values of the added mass in the pods. The main effect is – not surprisingly – to lower all the natural frequencies of the structure, moving the first flexion frequency of the wing towards the flexible goal of 3 Hz. The order of the modes is not affected, while it can observed a drift between the symmetric and antisymmetric torsion modes.

In the following, a mass of $2 \times 2.0\,\text{kg}$ at each wing tip is considered in order to obtain a first natural frequency that satisfy the specifications. Even if a larger mass could fit in the pods – i.e. $2 \times 2.5\,\text{kg}$ – we prefer to allow ourselves some margin to adjust the performance of the aircraft after its fabrication and the assessment of its real dynamic behaviour during the ground vibration test (GVT) campaign.

4.2 Flutter in the flight domain (position of the tip masses and ply angle)

Differently from a classical aeroelastic design, we aim – for one of the configurations – to onset the flutter in the flight domain. This can be achieved by changing the organisation of the natural vibration modes and, consequently, having them interacting in a suitable way. A classical flutter mechanism sees usually the coupling of a flexion mode with a torsion one; since the position of the flexion modes is prescribed by the specifications, we choose to *move* the torsional one and, hence, allow the aeroelastic coupling.

In order to achieve this, we change the position of the masses in the pods at the wing tips. By increasing the distance d_{tip} between the two masses, we can add torsional inertia to the wing and, thus, decrease the frequency of the natural torsion modes. Figure 7(top) reports the evolution of the modal organisation as a function of this distance: as expected, we are able to bring the frequencies of torsion modes closer to those of bending modes. The effects on the flutter behaviour are shown in Figure 7(bottom); the height of the bars indicates the value of the critical flutter speed, while the colours the modal contributions – as in Figure 5(right) – for the critical mode. If no flutter is detected within the investigated range of velocity, no bars are reported. The configuration with centred masses exhibits an antisymmetric flutter at the VNE, while we find again the coplanar mechanism of the baseline configuration for the first step of d_{tip}. For $d_{tip} = 0.2\,\text{m}$, the torsional modes are isolated in the frequency range and, hence, no flutter instability is detected. Increasing the distance, we find the desired symmetric mechanism

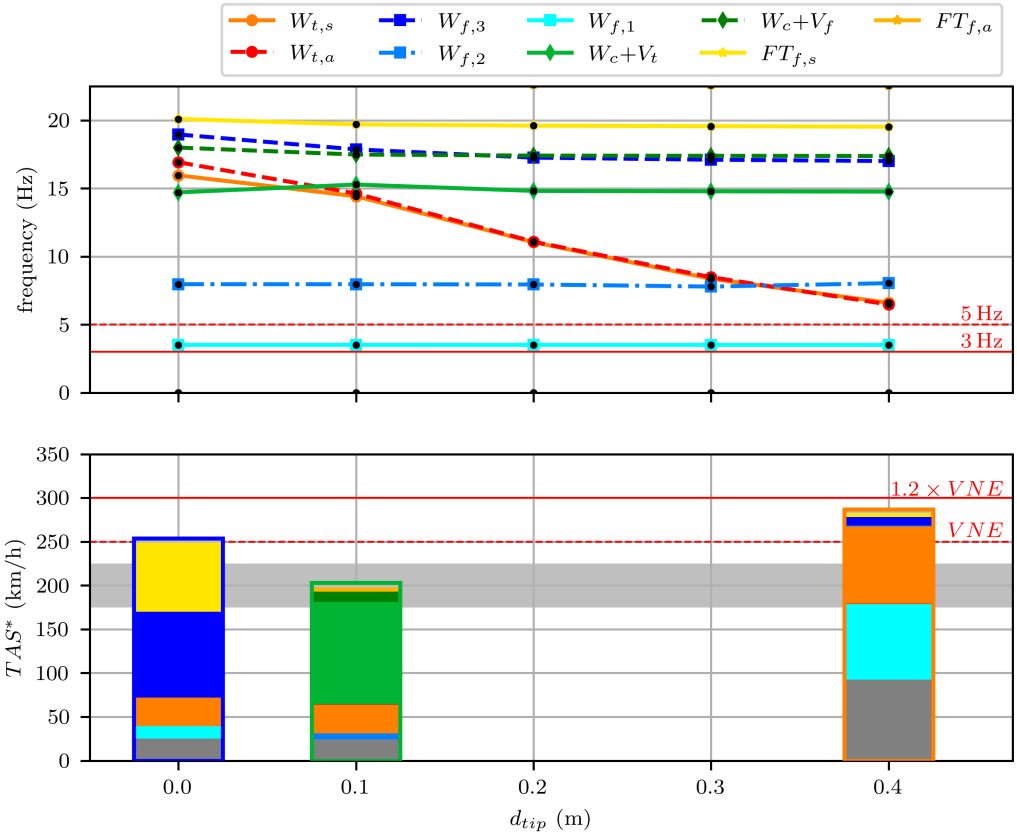

Figure 7: Parametric study on the position of the mass at the wing-tip (d_{tip}). The values of the other design parameters are: $\theta_{ply} = -45°$, $m_{tip} = 2\,\text{kg}$, and $m_{ft} = 0\,\text{kg}$.

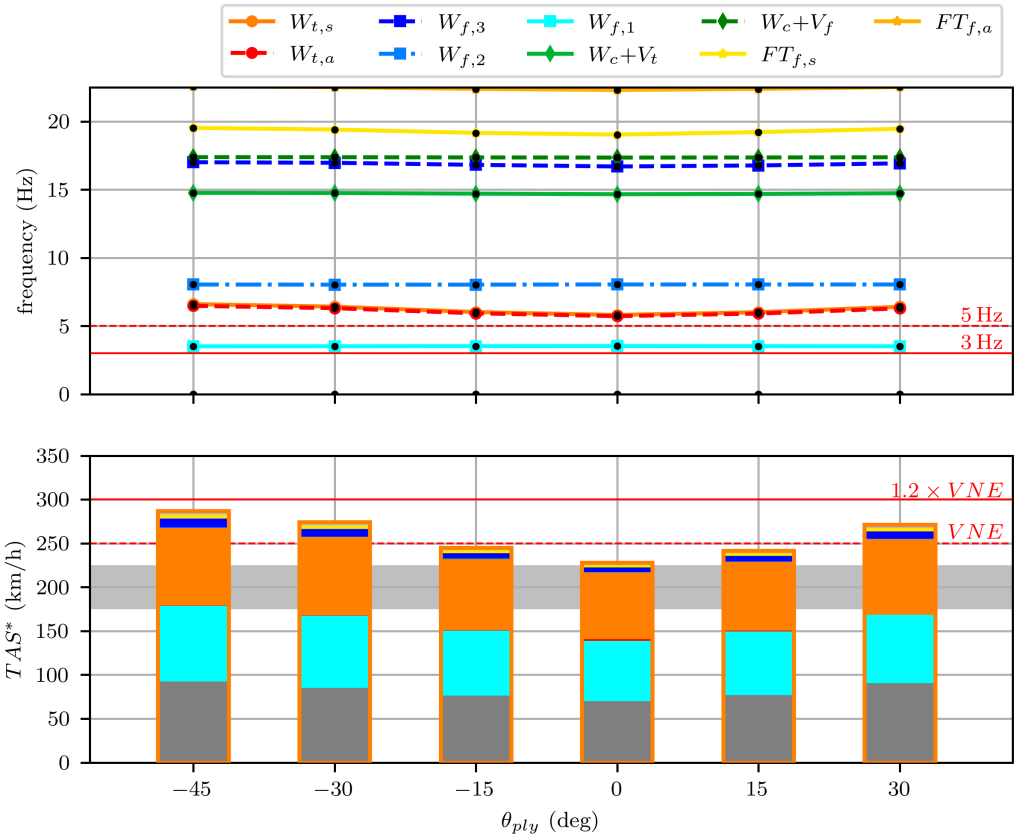

Figure 8: Parametric study on the mid-ply angle (θ_{ply}). The values of the other design parameters are: $m_{tip} = 2\,\text{kg}$, $d_{tip} = 0.4\,\text{m}$, and $m_{ft} = 0\,\text{kg}$.

for a distance of $0.4\,\text{m}$; in this case, the two torsional modes sit between the first and second flexion modes, allowing the coupling of the symmetrical ones. However, the critical flutter velocity is not in the required range, reported by the horizontal grey area.

We leverage the mid-ply angle θ_{ply} to bring closer the first flexion and the symmetric torsion modes, in order to promote their coupling and, hopefully lower the critical flutter speed. By changing this parameter, in fact, we can reduce the torsional stiffness of the wing in favour of the flexion one; this effect can be clearly seen in Figure 8(top). The critical flutter velocity reported in Figure 8(bottom) shows the desired effect on the critical velocity. At $\theta_{ply} = 0°$ – i.e. all the skin plies with the same orientation along the span – we almost achieve the required range of flutter speed; however, this would mean that the torsional rigidity of the wing would be given only by the matrix phase of the composite material, compromising the structural safety of the structure. Because of this reason, we will continue with our design with a safer value of $\theta_{ply} = +15°$, to comply with the specifications thanks to the last design parameter, i.e. the mass of the flutter tuner.

4.3 Fine tuning of the flutter behaviour (flutter tuner)

The current configuration ($\theta_{ply} = +15°$, $m_{tip} = 2\,\text{kg}$, and $d_{tip} = 0.4\,\text{m}$) allows a critical flutter speed close to – but not yet within – the specifications.

We can comply with the requirements of the flutter configuration by increasing the mass of the flutter tuner (m_{ft}). This allows to further displace the torsion modes towards the first flexion one without any effect on the flexion modes frequency (Figure 9, top). This results in promoting the flutter onset, as reported in Figure 9(bottom). Already for $m_{ft} = 0.4\,\text{kg}$ the critical flutter speed adheres to the specifications, reaching the lower limit of the flutter range for $m_{ft} = 1.0\,\text{kg}$.

The role of the flutter tuner is not only to promote flutter, but also to avoid it. Its effect on the modal scenario can allow to prevent the coupling between modes and, thus, disable the flutter mechanism. This is the case for the candidate to the flexible configuration ($\theta_{ply} = +15°$, $m_{tip} = 2\,\text{kg}$, and $d_{tip} = 0\,\text{m}$), that is required to be flutter stable in the extended flight domain. As reported in Figure 10(a), without mass in the flutter tuner it presents a critical flutter speed within the flight domain; however, a small mass in the flutter tuner ($m_{ft} = 0.2\,\text{kg}$) allows to prevent the onset of the flutter mechanism and, hence, comply with the specifications. This is not required for the candidate to the rigid configuration ($\theta_{ply} = +15°$ and $m_{tip} = 0\,\text{kg}$), which is already flutter stable for $m_{ft} = 0\,\text{kg}$, see Figure 10(b).

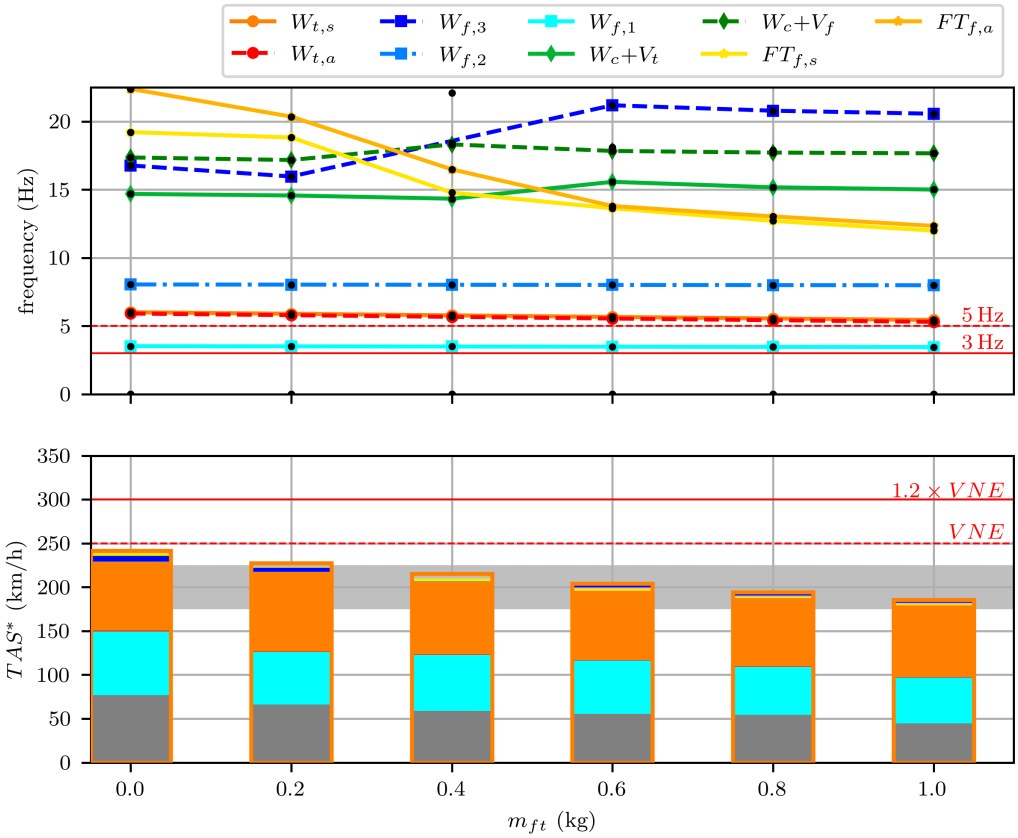

Figure 9: Parametric study on the mass in the flutter tuner (m_{ft}). The values of the other design parameters are: $\theta_{ply} = +15°$, $m_{tip} = 2\,\text{kg}$, and $d_{tip} = 0.4\,\text{m}$.

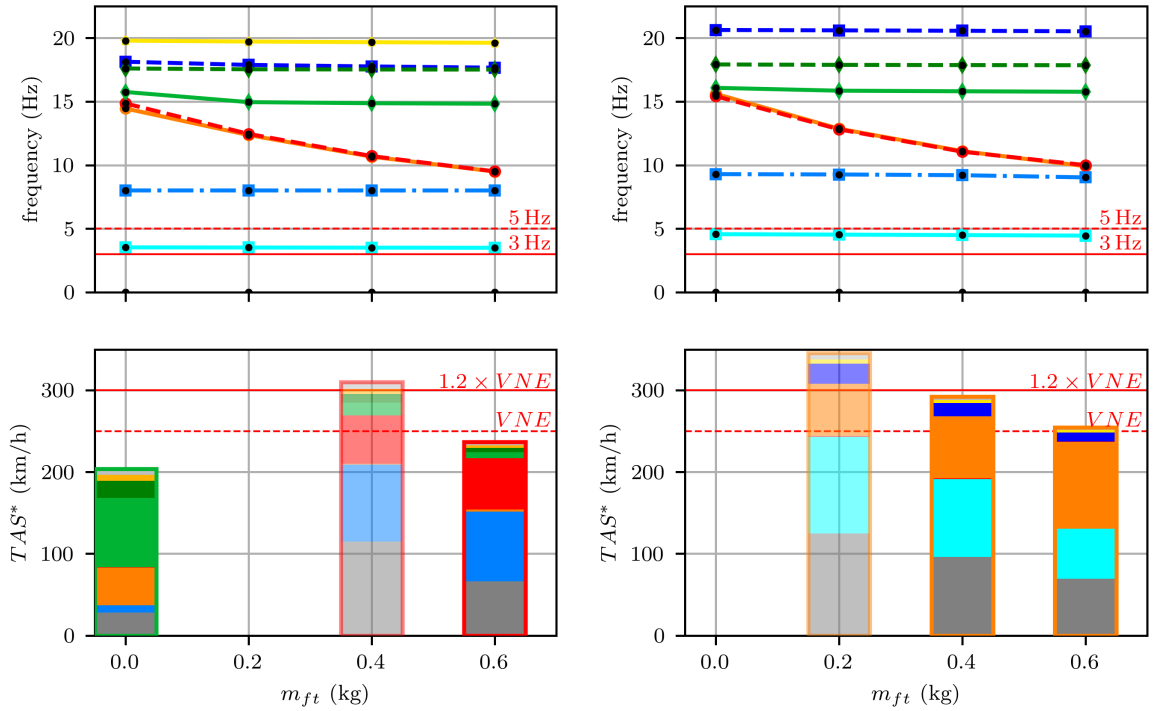

(a) Flexible configuration: $m_{tip} = 2\,\text{kg}$.

(b) Rigid configuration: $m_{tip} = 0\,\text{kg}$.

Figure 10: Parametric study on the mass in flutter tuner (m_{ft}) for the flexible (a) and the rigid (b) configurations. The values of the other design parameters are: $\theta_{ply} = +15°$ and $d_{tip} = 0\,\text{m}$.

5 FINAL CONFIGURATIONS

This section summarises the design identified in § 4 that comply with the specifications in § 2. The value of the design parameters for the three required configurations are reported in Table 3. They all share the same structure ($\theta_{ply} = 15°$) and the different behaviours (rigid, flexible, and flutter) are obtained only by changing the value (m_{tip} and m_{ft}) and position (d_{tip}) of the adjustable masses. Figure 11 resumes the modal organisation of the identified configurations, as well as the critical flutter velocity. The rigid and flexible configurations are flutter stable, with a first natural mode of 4.57 Hz and 3.52 Hz respectively. The flutter configuration, instead, presents a critical flutter speed of 185.5 km/h, within the velocity range specified in the design objectives.

Flutter sensitivity to structural damping. The error-bars in Figure 11(bottom) report the flutter speed taking into account a 1.5% structural damping. As expected, this has the effect to delay the flutter onset toward higher speeds; if this could be beneficial for the flutter stable configuration, it is detrimental to the flutter one. Nevertheless, the critical velocity remains within the specifications also when the structural damping is considered.

Table 3: Design parameters and performance of the identified configurations (rigid, flexible and flutter). The values for the baseline configuration are also reported as for reference.

Label	θ_{ply}	m_{tip}	d_{tip}	m_{ft}	f_1^n	TAS^*
baseline	$-45°$	–	–	–	$f_{f,1}^w = 4.55$ Hz	268.6 km/h
rigid	$+15°$	–	–	–	$f_{f,1}^w = 4.57$ Hz	> 350 km/h
flexible	$+15°$	2×2.0 kg	± 0.0 m	0.2 kg	$f_{f,1}^w = 3.52$ Hz	> 350 km/h
flutter	$+15°$	2×2.0 kg	± 0.4 m	1.0 kg	$f_{f,1}^w = 3.46$ Hz	185.5 km/h

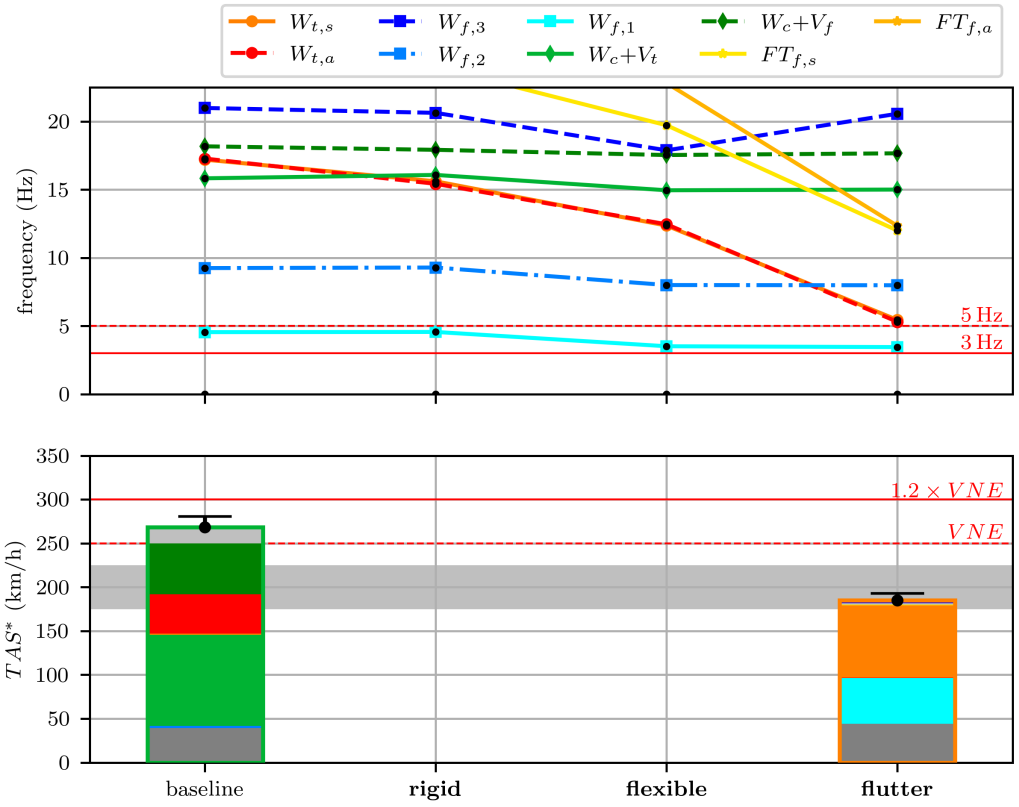

Figure 11: Synthesis of the dynamic and aeroelastic characteristics of the baseline and the three identified configurations (rigid, flexible and flutter, see Table 3).

5.1 Verification of the other aeroelastic constraints

The design requirements (see § 2) specify also some standard constraints on the aeroelastic behaviour of the aircraft. These concern the control reversal and the aeroelastic wing deformation.

Control reversal. The three configurations do not exhibit control reversal in the extended flight domain, i.e. $TAS \leq 1.2 \times VNE = 300\,\text{km/h}$. Figure 12 reports the aeroelastic effectiveness of the control surfaces, defined as the ratio between the aeroelastic and rigid control derivatives. The roll moment coefficient is considered for the ailerons, while yaw and pitch for the rudder and elevator respectively. The analysis confirms that a control effectiveness of at least 70% is ensured in the flight domain.

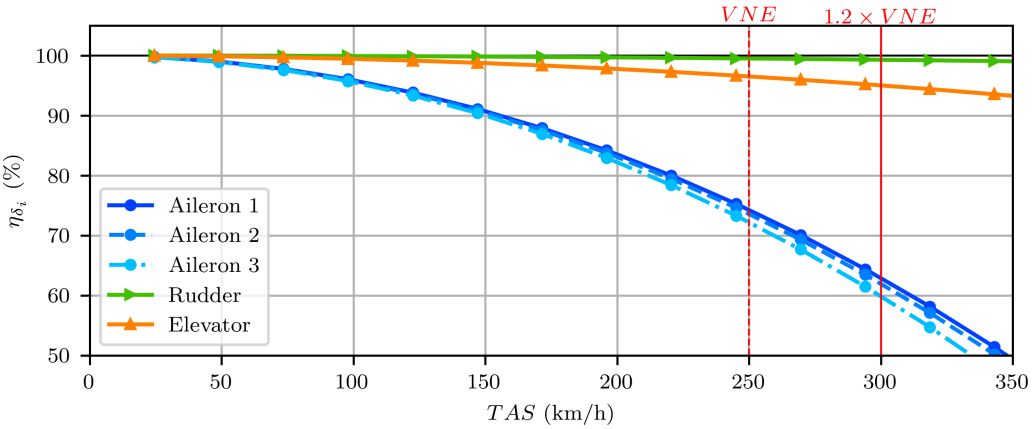

Figure 12: Aeroelastic effectiveness of the control surfaces for the final design.

Aeroelastic twist and displacement. The aeroelastic static displacement is computed for the trim conditions listed in Table 4. Along the cruise condition, symmetric, trimmed manoeuvres with positive and negative load-factors are considered (TURN+ and TURN-). A gust condition is taken into account by adding the untrimmed flight condition ΔGUST to the cruise load. Similarly a roll manoeuvre is considered at the maximum expected roll rate of the aircraft. The aeroelastic displacement and twist are reported in Figure 13 for the three mass configurations. The twist at cruise condition respects the specification, remaining below $1°$. The adjustable masses have the expected effect on the aeroelastic static behaviour of the wing: an additional mass at the wing-tip unloads the wing, resulting in a lower displacement. On the other hand, the twist exhibits the opposite behaviour, specially when the tip masses are decentred with respect to the pod centre (flutter configuration, $d_{tip} = 0.4\,\text{m}$). The structural integrity to the here-presented load cases is currently being verified at ONERA.

Table 4: Aeroelastic load cases.

Label	Load factor	Roll-rate	Trim variables
CRUISE	$+1.0\,\text{g}$	$0°/\text{s}$	AoA, δ_e
TURN+	$n_{turn,pos} > 0$	$0°/\text{s}$	AoA, δ_e
TURN-	$n_{turn,neg} < 0$	$0°/\text{s}$	AoA, δ_e
ΔGUST	$n_{gust} - 1.0\,\text{g} > 0$	$0°/\text{s}$	AoA
ΔROLL	$+0.0\,\text{g}$	$\dot{\theta}_{x,max\ roll}$	$\delta_{a,1} = \delta_{a,2} = \delta_{a,3}$

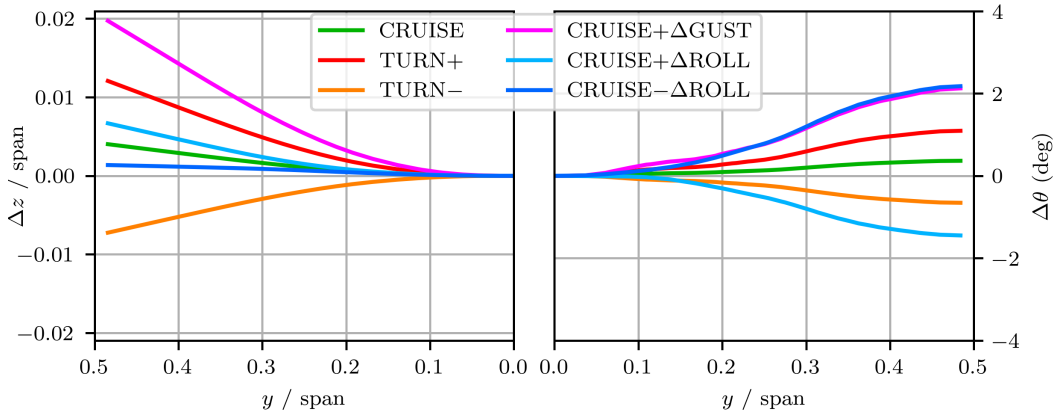

(a) Rigid configuration.

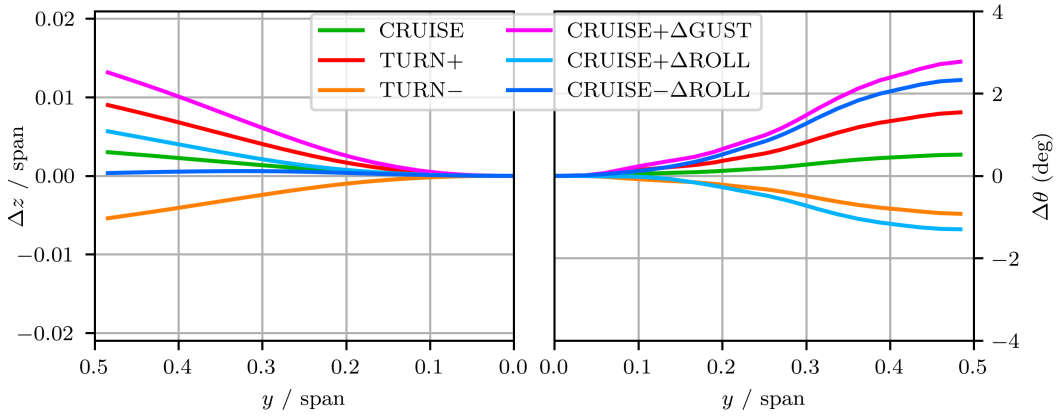

(b) Flexible configuration.

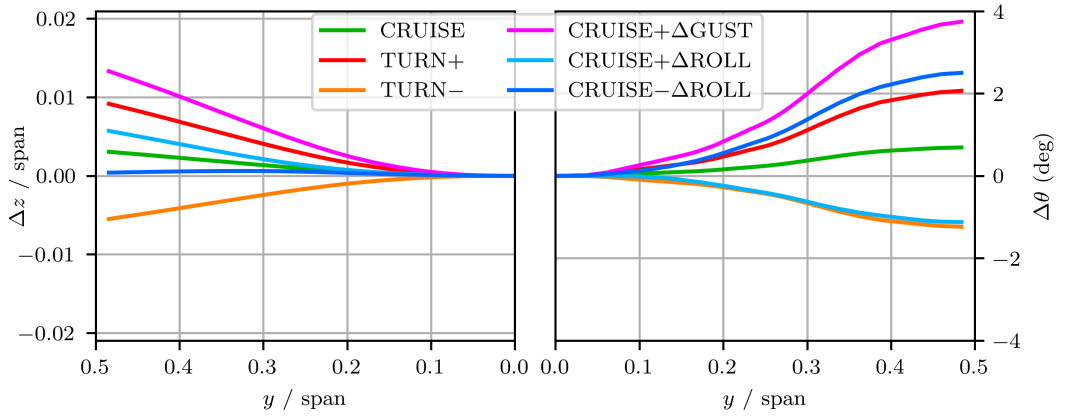

(c) Flutter configuration.

Figure 13: Aeroelastic displacement (Δz, left) and twist ($\Delta\theta$, right) for the three identified configurations subjected to the trim conditions listed in Table 4.

6 CONCLUSIONS

The aeroelastic design problem of an unmanned, remote-controlled aircraft for the experimental test of active flutter control is presented. The peculiar mission of the aircraft led to unconventional specifications (§ 2), namely the onset of flutter within the flight domain. Moreover, three configurations (rigid, flexible, and flutter) are required to gradually approach the flutter control, with increasing levels of aeroelastic coupling and, hence, operating risks during the flight-test campaigns. These are required to share the same wing structure, leaving the control of the aeroelastic behaviour only to ground-adjustable masses.

The overall configuration of the Experimental Validation Aircraft (EVA) is presented, and the design parameters are introduced (§ 3). These consist in adjustable masses – two at each wingtip and one at the end of a rear-facing beam on the wing – and the orientation of the midply of the composite skin of the wing. The aeroelastic design is thus addressed (§ 4). Each parameter is tuned to comply with the design objectives by means of consecutive parametric studies. Finally, the three required configurations are presented and additional, conventional aeroelastic constraints (control reversal and aeroelastic twist) are verified (§ 5).

The proposed design is currently undergoing structural verification at ONERA. If validated, it will be manufactured by Aviation Design, to take part to the joint flight-test campaign within the Clean Aviation project CONCERTO.

7 REFERENCES

[1] Munk, M. (1949). Propeller containing diagonally disposed fibrous material. U.S. Patent 2,484,308,1111.

[2] Shirk, M. H., Hertz, T. J., and Weisshaar, T. A. (1986). Aeroelastic tailoring - theory, practice, and promise. *Journal of Aircraft*, 23(1).

[3] Jutte, C. and Stanford, B. (2014). Aeroelastic tailoring of transport aircraft wings: State-of-the-art and potential enabling technologies. Technical Report NASA/TM-2014-218252, NASA.

[4] Arizono, H. and Isogai, K. (2005). Application of genetic algorithm for aeroelastic tailoring of a cranked-arrow wing. *Journal of Aircraft*, 42(2), 493–499.

[5] Dillinger, J. K. S. (2014). *Static aeroelastic optimization of composite wings with variable stiffness laminates*. Phd thesis, TU Delft, The Netherlands.

[6] Fabbiane, N., Irisarri, F.-X., Dillinger, J., et al. (2022). Aeroelastic-tailoring of a wind-tunnel model for passive alleviation of static and dynamic loads. *CEAS Aeronaut. J.*, 13(4), 967–977. doi:10.1007/s13272-022-00615-0.

[7] Hertz, T. J., Shirk, M. H., Ricketts, R. H., et al. (1981). Flutter suppression using active controls based on the concept of aerodynamic energy. Technical Report AFWAL-TR-81-3043, Air Force Wright Aeronautical Labs.

[8] Bisplinghoff, R. L., Ashley, H., and Halfman, R. L. (1996). *Aeroelasticity*. Dover Publications. ISBN 9780486691893.

[9] Scarth, C. and Cooper, J. E. (2018). Reliability-based aeroelastic design of composite plate wings using a stability margin. *Structural and Multidisciplinary Optimization*, 57, 1695–1709.

[10] Coelho, L. (2023). *Reliability-based design optimization of composite laminates for aeroelastic applications*. Phd thesis, Université Paris-Saclay, France.

[11] Coelho, L., Fabbiane, N., Fagiano, C., et al. (2022). Gradient reliability-based design optimization of a composite plate through multi-scale design spaces. In *Proceedings of the 19th International Forum on Aeroelasticity and Structural Dynamics*. Madrid, Spain.

[12] Nissim, E. (1971). Flutter suppression using active controls based on the concept of aerodynamic energy. Technical Report NASA/TN-D-6199, NASA.

[13] Livne, E. (2018). Aircraft active flutter suppression: State of the art and technology maturation needs. *Journal of Aircraft*, 55(1), 410–452. doi:10.2514/1.C034442.

[14] Takarics, B., Patartics, B., Luspay, T., et al. Active flutter mitigation testing on the flexop demonstrator aircraft. In *Proceedings of the AIAA Scitech 2020 Forum*. doi:10.2514/6.2020-1970.

[15] Ricci, S., Marchetti, L., Riccobene, L., et al. (2021). An Active Flutter Suppression (AFS) project: Overview, results and lessons learned. In *Proceedings of the AIAA Scitech 2021 Forum*. doi:10.2514/6.2021-0908.

[16] Vanek, B., Bodor, V., Takarics, B., et al. (forthcoming). Aeroelastic aircraft design and flight control methods applicable for flutter suppression: The FLIPASED perspective. In *Proceedings of the 20th International Forum on Aeroelasticity and Structural Dynamics*. The Hague, The Netherlands.

[17] MSC Software (2023). *MSC Nastran Design Sensitivity and Optimization User's Guide*.

[18] Hassig, H. J. (1971). An approximate true damping solution of the flutter equation by determinant iteration. *Journal of Aircraft*, 8(11), 885–889. doi:10.2514/3.44311.

ACKNOWLEDGEMENTS

This work have been conducted within the project CONCERTO (Construction Of Novel CERTification methOds and means of compliance for disruptive technologies), funded by the EU Clean Aviation Joint Undertaking program (Grant Agreement No. 101101999).
Project's website: `https://www.concertoproject.eu/`

The authors would like to acknowledge the other partners of the project, especially Elsa Breus, Olivier Valsecchi, Pierre Bassignac, and Eric Garrigues from Dassault Aviation and Eric Rantet from Aviation Design for the fruitful discussions and collaboration.

COPYRIGHT STATEMENT